Exploring the Role of Eddy Momentum Fluxes in Determining the Characteristics of the Equinoctial Hadley Circulation: Fixed-SST Simulations

MARTIN S. SINGH AND ZHIMING KUANG

Department of Earth and Planetary Sciences, Harvard University, Cambridge, Massachusetts

(Manuscript received 27 July 2015, in final form 12 February 2016)

ABSTRACT

The influence of eddy momentum fluxes on the equinoctial Hadley circulation is explored using idealized simulations on an equatorial beta plane in which the sea surface temperature (SST) distribution is fixed. By comparing simulations run in a wide-domain configuration, in which large-scale eddies are present, to simulations in which the model domain is too narrow to permit baroclinic instability, the role of large-scale eddies in determining the characteristics of the Hadley circulation is elucidated. The simulations also include an explicit representation of deep convection, allowing for an evaluation of the influence of convective momentum transport on the zonal-mean circulation.

The simulated eddy momentum fluxes are much weaker in the narrow-domain configuration than in the wide-domain case, and convective momentum transport is found to be of secondary importance. As a result, many characteristics of the narrow-domain Hadley circulation are well described by axisymmetric theory and differ from those of the wide-domain case. Nevertheless, the strength of the Hadley circulation is similar irrespective of the domain width. The sensitivity of this result to the strength of the eddy forcing is investigated using narrow-domain simulations forced by artificial sinks of zonal momentum. As the magnitude of the momentum sink increases, the Hadley circulation strengthens, but the increase is relatively modest except at very strong forcing magnitudes. The results suggest that the fixed-SST boundary condition places a strong thermodynamic constraint on the Hadley circulation strength and that one should consider the energy budget as well as the angular momentum budget in order to fully understand the influence of large-scale eddies on the zonal-mean circulation in the tropics.

1. Introduction

While it has long been recognized that Earth's Hadley circulation (HC) is influenced by the momentum transports associated with large-scale eddies, theoretical understanding of the relationship between the eddy fluxes and the strength of the tropical overturning remains incomplete. One approach to the problem is to consider the HC as a response to imposed sources of heat and momentum owing to eddies and diabatic effects either diagnostically, using the Kuo–Eliassen equation (Eliassen 1951; Kuo 1956), or with a dynamical model (e.g., Dickinson 1971; Schneider 1984). Kuo (1956) used this framework to suggest that the bulk of the HC mass flux is associated with eddy momentum fluxes rather than radiative cooling. Studies that include the effect of latent heat release in cumulus clouds, however, point to a more modest role for the eddies (e.g., Dickinson 1971; Krishnamurti et al. 2013). Moreover, this approach is limited in that it cannot account for the feedback between changes in eddy fluxes and changes in the circulation, potentially resulting in an underestimate of the importance of eddies for the mean flow (Kim and Lee 2001).

More recent work has compared the HC simulated by axisymmetric (2D) and three-dimensional (3D) models in order to understand how the circulation is affected by the presence of eddies (e.g., Williams 1988a,b). Many such studies have found the potential for substantial amplification of the equinoctial HC in 3D relative to the 2D case (Becker et al. 1997; Kim and Lee 2001; Walker and Schneider 2005). An exception is the work of Satoh et al. (1995, hereafter S95), who found that the HC strength increased only slightly in eddy-permitting simulations relative to the axisymmetric case (see also Satoh 1994). An important distinction is that S95

Corresponding author address: Martin S. Singh, Department of Earth and Planetary Sciences, Harvard University, 20 Oxford St., Cambridge, MA 02138.
E-mail: martinsingh@fas.harvard.edu

DOI: 10.1175/JAS-D-15-0212.1

imposed a fixed distribution of sea surface temperature (SST) in their simulations, while the other studies mentioned above enforce an energetically closed boundary condition. In this paper, we build on the work of S95 and investigate the role of eddy momentum fluxes in determining the characteristics of the equinoctial HC under fixed-SST conditions.

Theories of the HC often focus on one of two limits: the linear viscous limit, in which frictional processes balance the Coriolis torque on the upper-tropospheric flow (e.g., Schneider and Lindzen 1976, 1977), and the nonlinear angular momentum–conserving limit, in which the Coriolis torque is balanced by mean-flow advection (e.g., Schneider 1977; Held and Hou 1980; Lindzen and Hou 1988; Satoh 1994; Fang and Tung 1996, 1999; Caballero et al. 2008). In the former limit, the HC strength is related to the magnitude of the frictional momentum sink in the subtropics; in the axisymmetric studies of Schneider and Lindzen (1976, 1977), this refers to frictional torques associated with cumulus convection. But the momentum sink could also be provided by large-scale eddy fluxes. The HC strength in the angular momentum–conserving limit, on the other hand, is directly controlled by the thermal driving.

Walker and Schneider (2006) examined the proximity of the atmosphere to each of these limits in a series of idealized simulations of the equinoctial HC with a general circulation model (GCM). They considered a steady-state balance equation for the strength of the meridional flow in the upper troposphere based on the angular momentum budget given by

$$f\overline{v}(1-\mathrm{Ro}_L)\approx -s. \tag{1}$$

Here, f is the Coriolis parameter, v is the meridional velocity, s is the convergence of the eddy flux of zonal momentum, $\mathrm{Ro}_L=-\overline{\zeta}/f$ is the local Rossby number, with ζ being the relative vorticity, and the overbar represents a zonal and time mean. Equation (1) neglects friction and vertical advection of angular momentum by the mean flow; but it may be applied in the upper troposphere near the latitude of the streamfunction maximum, where the flow is quasi horizontal and frictional torques are presumed to be small.

In the linear limit, $\mathrm{Ro}_L \ll 1$, nonlinear advection of angular momentum by the mean flow is weak, and the above equation provides a direct relationship between the strength of the meridional flow in the upper troposphere and the eddy momentum flux divergence. In the weak eddy limit, on the other hand, angular momentum is conserved in the HC, $\mathrm{Ro}_L \approx 1$, and (1) provides no information about the meridional flow. Walker and Schneider (2006) conducted simulations over a wide range of parameters and found that, in most cases, the equinoctial HC remained relatively close to the low-Rossby-number, linear regime ($\mathrm{Ro}_L \lesssim 0.4$), and the HC strength varied roughly in proportion to a measure of the subtropical eddy momentum flux divergence.

Earth's HC lies between the linear and angular momentum–conserving limits; the Rossby number at the center of the HC varies from ~0.2 in the summer cell to $\gtrsim$0.5 in the winter cell (Schneider and Bordoni 2008). While a comprehensive theory for the HC in the intermediate-Rossby-number regime remains elusive, a number of authors have appealed to the angular momentum budget in order to understand variations in the HC strength over the seasonal cycle (Walker and Schneider 2005; Schneider and Bordoni 2008; Bordoni and Schneider 2008, 2010) and variations in the strength of the winter cell on interannual time scales (Caballero 2007) and across different climate models (Caballero 2008). In this study, we consider idealized simulations of an equinoctial HC in a regime where nonlinear advection of angular momentum by the mean flow is important.

Previous modeling studies investigating the importance of eddies for the HC are primarily based on simulations with GCMs in which the effects of moist convection, including its effect on the momentum budget, must be parameterized. In idealized simulations, such as those of Walker and Schneider (2006), convective momentum transport is typically neglected. But it is known that momentum transport by moist convection can be important for the strength (Zhang and McFarlane 1995) and seasonal cycle (Wu et al. 2003) of the HC. Here, we use the diabatic acceleration and rescaling (DARE) approach of Kuang et al. (2005) in order to conduct idealized simulations of an equinoctial HC with an explicit representation of moist convection. The DARE approach reduces the scale separation between convection and the large-scale flow and allows deep convection to be simulated explicitly at reasonable computational cost, albeit with some distortions. This enables an evaluation of the importance of momentum transport by deep convection for the HC. Smaller-scale eddies associated with shallow convection and boundary layer turbulence are not well resolved in these simulations, but for simplicity we do not employ an explicit boundary layer or shallow convection parameterization.

We simulate the HC on an equatorial beta plane in two configurations: a wide domain, in which large-scale eddies are present, and a narrow domain, in which baroclinic instability does not occur, and only eddies at the mesoscale or smaller are permitted. These model configurations allow us to isolate the effect of large-scale eddies on the HC. We consider the simple case of a fixed-SST lower boundary with a range of different pole-to-equator temperature

gradients. The HC in the wide domain has a lower Rossby number than in the narrow domain, reflecting the stronger effect of eddy momentum fluxes, but the HC strength is nonetheless similar between the two cases. Using an approach similar to that of Schneider (1984), we also consider narrow-domain simulations in which the effects of eddy momentum fluxes are included as a direct tendency on the zonal wind; as the forcing magnitude increases, the HC strengthens, but the HC strength does not increase proportionally to the imposed momentum forcing. The importance of the SST distribution for the HC strength in our simulations suggests that one should consider the energy budget as well as the momentum budget in order to fully understand the effect of eddies on the HC.

The rest of this paper is organized as follows: We first describe the model configuration and simulations used (section 2) before examining the mean circulation and angular momentum transports in the wide-domain and narrow-domain configurations (section 3). Next, we consider the sensitivity of the circulation to the magnitude of the eddy fluxes in narrow-domain simulations with imposed eddy momentum flux divergences (section 4). Finally, we give a summary of our conclusions and their implications (section 5).

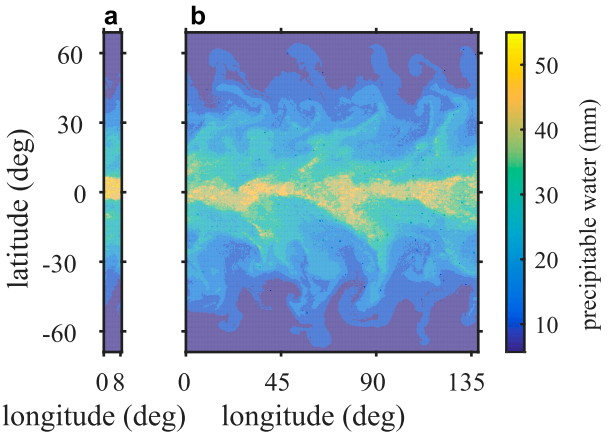

FIG. 1. Snapshot of total precipitable water for the (a) narrow-domain simulation (24×384 grid points) and (b) wide-domain simulation (384×384 grid points) with $\Delta T = 40$ K and idealized radiation scheme based on Newtonian relaxation. Domains are shown with a one-to-one aspect ratio.

2. Idealized Hadley circulations on an equatorial beta plane

a. Model configuration

We consider simulations of an idealized equinoctial HC using version 6.9.5 of the System for Atmospheric Modeling [SAM; Khairoutdinov and Randall (2003)]. The model integrates prognostic equations for the frozen moist static energy (FMSE), total precipitating water, total nonprecipitating water, and three velocity components under the anelastic approximation. Within the model's thermodynamic formulation, FMSE is conserved for adiabatic motions, including condensation and freezing. A simple one-moment formulation of cloud and precipitation microphysics is used, and subgrid-scale motions are parameterized using a 1.5-order scheme that includes a prognostic equation for the subgrid-scale turbulence kinetic energy. Surface fluxes of sensible heat, latent heat, and momentum are computed using bulk aerodynamic formulas with turbulent exchange coefficients derived from Monin–Obukhov similarity theory and dependent on the near-surface wind speed and near-surface gravitational stability. The effect of subgrid-scale wind variability on the surface fluxes is parameterized by enforcing a minimum value of 1 m s^{-1} on the wind speed used in the surface flux calculation. While our model resolution is not sufficient to accurately simulate boundary layer eddies, we do not use an explicit boundary layer parameterization beyond the Monin–Obukhov scheme described above.

Simulations are run on an equatorial beta plane extending from 68°S to 68°N, with solid walls (free-slip boundary condition) at the northern and southern boundaries and with periodic boundary conditions in the zonal direction. The zonal width of the domain is either 9° (narrow) or 136° (wide) of longitude, depending on whether we wish to include the effects of large-scale eddies (Fig. 1). Here, we refer to disturbances with a characteristic length scale greater than ~1000 km as "large scale" and smaller-scale eddies as "mesoscale" or "small scale." Simulations in the wide domain support baroclinic instability and the resultant synoptic-scale eddies (although certain planetary-scale waves are excluded by the finite width), while in the narrow-domain case, only smaller-scale eddies related to moist convection are present. The simulations are run with 46 vertical levels, in which the vertical grid spacing varies between 100 m near the surface, 600 m in the mid- to upper troposphere, and 1000 m at the model top, which is set at 26.9 km. A sponge layer, with damping applied to the velocity fields, is included above 19 km to prevent gravity wave reflection.

b. DARE approach

Computational resource limits prevent us from performing the simulations described above on a fine-enough horizontal grid to fully resolve moist convection. Instead, we employ the DARE approach introduced by Kuang et al. (2005) in order to retain an explicit representation of moist convection at reasonable computational cost. Under

DARE, the scale separation between convection and large-scale motions is reduced by altering physical parameters within the system. In particular, the DARE approach involves 1) reducing the radius of Earth by a factor γ, 2) increasing the rotation rate of Earth by the same factor, and 3) reducing the time scales of diabatic processes (e.g., radiative and microphysical processes) also by the factor γ. Here, we use a value of $\gamma = 10$, which results in a decrease in the computational costs relative to a full-resolution simulation by a factor of order $\gamma^3 = 1000$. For our beta-plane simulations, the first two alterations used in the DARE approach are achieved by changing β, the gradient of the Coriolis parameter in the meridional direction, while the third alteration is achieved by increasing the tendencies resulting from diabatic processes, such as radiative heating and cooling, surface fluxes, condensation and evaporation, and precipitation fallout. Our simulations are run with an effective horizontal grid spacing of 40 km. This means that, when scaled back to the length and time scales appropriate for Earth, the horizontal grid spacing is 40 km. But since we use a DARE factor $\gamma = 10$, the grid spacing relevant for moist convection is 4 km.

The DARE approach is mathematically equivalent to the hypohydrostatic rescaling outlined in Pauluis et al. (2006) [referred to as reduced acceleration in the vertical in Kuang et al. (2005)], in which the physical parameters of the system are unchanged but the vertical momentum equation is altered by increasing the magnitude of the inertia term by the factor γ. This formulation demonstrates that the effect of DARE is to increase the importance of nonhydrostatic motions at mesoscales but to leave large-scale hydrostatic motions unaltered. In particular, the ratio of the Rossby radius to Earth's radius remains fixed under the DARE approach. Thus, to the extent that large-scale atmospheric dynamics are unaffected by nonhydrostatic motions, the DARE approach does not alter the dynamics of large-scale eddies when the solution is scaled back to the length and time scales appropriate for Earth.

Pauluis et al. (2006) showed that the hypohydrostatic rescaling results in a slowdown of the convective life cycle and that this can result in unrealistic distributions of cloud liquid and ice in simulations of radiative–convective equilibrium. In our simulations, we exclude cloud-radiative interactions (see below), and we find that the mean circulation and HC strength of a narrow-domain simulation is very similar when using the DARE approach ($\gamma = 10$, grid spacing = 40 km) compared to when running at full resolution ($\gamma = 1$, grid spacing = 4 km). A more detailed evaluation of the DARE approach applied to our simulations is presented in the appendix.

c. Simulation design

We conduct simulations in which the surface temperature T_s is prescribed as a zonally symmetric function of latitude with a maximum at the equator according to

$$T_s = T_0 - \Delta T \sin^2(\phi), \tag{2}$$

where ϕ is latitude, T_0 is set to 300 K, and simulations are conducted with values of ΔT in the range 10–100 K. For ease of interpretation, we parameterize the effects of radiative heating and cooling through a simple Newtonian relaxation to a fixed temperature. Specifically, the temperature tendency owing to radiation is given by

$$\left.\frac{\partial T}{\partial t}\right|_{\text{rad}} = -\frac{T - T_R}{\tau}, \tag{3}$$

with $T_R = 220$ K and $\tau = 50$ days. Note that (3) does not depend on the water vapor or cloud fields, and thus the effect of cloud and water vapor radiation feedbacks on the circulation are not included here. We also consider alternate simulations in which radiative transfer is parameterized using a two-stream gray scheme identical to that described in O'Gorman and Schneider (2008). The gray-radiation simulations allow for a stronger feedback between the atmospheric temperature structure and the radiative cooling rate (although cloud and water vapor feedbacks are still neglected). However, the HC strength in the gray-radiation simulations is substantially stronger than that of Earth's equinox conditions, and thus we focus on the Newtonian-relaxation simulations in this paper.

In all simulations, the atmosphere is initialized with horizontally invariant profiles of temperature and humidity reflective of the tropical atmosphere, with random perturbations to the temperature field to break the initial symmetry. Time-mean properties of the flow shown in Figs. 2–13 are calculated based on 6-hourly snapshots over days 50–250 of the simulations.

3. Comparison of wide- and narrow-domain simulations

We compare the wide-domain and narrow-domain simulations in order to examine the effect of large-scale eddies on the HC. Figure 2 shows properties of the mean state in the wide- and narrow-domain cases for a pole-to-equator SST difference $\Delta T = 40$ K. Both simulations exhibit strong subtropical jets associated with strong meridional temperature gradients, while the tropical atmosphere is characterized by weak temperature gradients and easterly winds at low levels near the equator

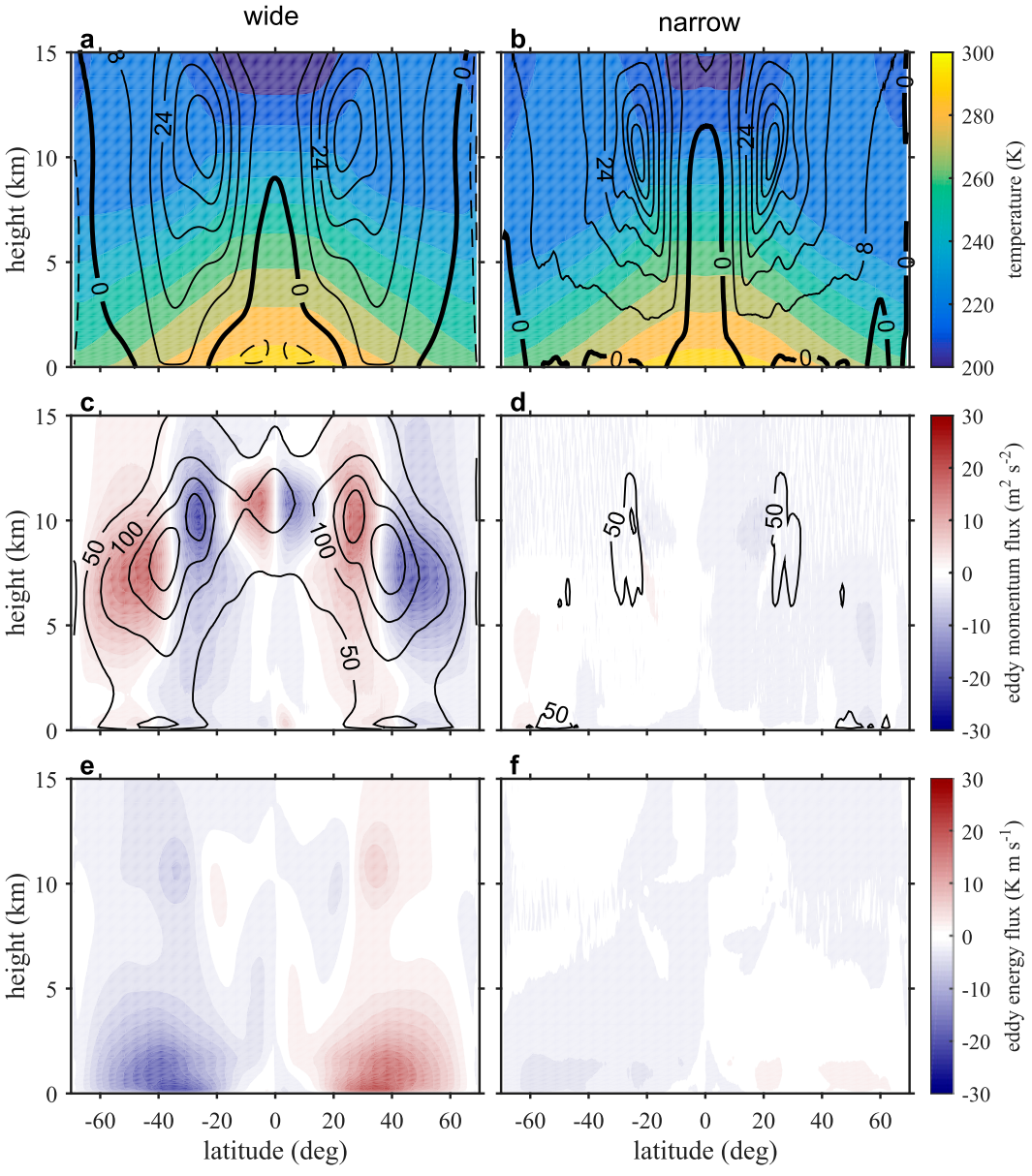

FIG. 2. Zonal- and time-mean properties of simulations with $\Delta T = 40$ K in the (left) wide and (right) narrow domains. (a),(b) Zonal wind (contours; dashed negative; zero contour is thick; m s^{-1}) and temperature (colors). (c),(d) Eddy kinetic energy per unit mass (contours; m^2 s^{-2}) and meridional eddy momentum flux $\overline{u'v'}$ (colors). (e),(f) Meridional eddy energy flux $1/c_p\overline{v'h'}$, where $h = c_pT + \Phi + L_vq$ is the moist static energy. Here, c_p is the isobaric specific heat capacity, T is the temperature, Φ is the geopotential, L_v is the latent heat of vaporization, and q is the specific humidity.

(Fig. 2a,b). The jets in the narrow-domain case are stronger and substantially sharper than in the wide-domain simulation. There is also a discernible mid-latitude jet in the wide-domain case associated with a nonzero surface zonal wind (Fig. 3), while in the narrow-domain case, the mean surface wind is close to zero. These features are consistent with weak eddy activity in the narrow-domain simulations; the eddy kinetic energy and meridional eddy fluxes of energy and momentum are substantially smaller in the narrow-domain simulations compared to the corresponding wide-domain case (Figs. 2c–f).

The mean circulation in the wide-domain simulation shown in Fig. 2 is broadly similar to that of Earth at the equinox, although the simulated subtropical jets are somewhat stronger than observed (e.g., Peixoto and

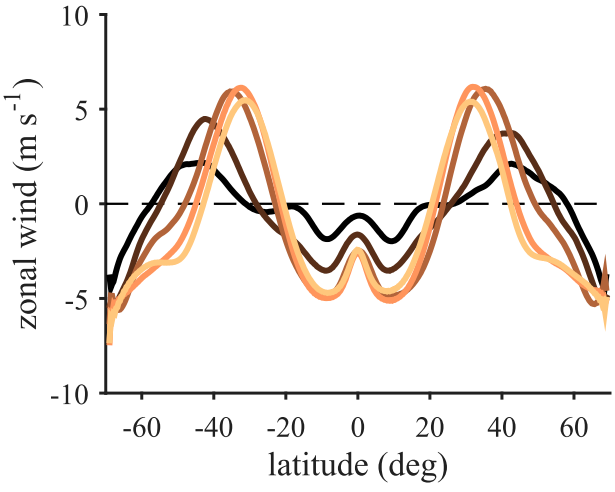

FIG. 3. Zonal- and time-mean zonal wind velocity at the lowest model level for wide-domain simulations with $\Delta T = 10$ (black), 20, 40, 80, and 100 K (orange). The dashed line shows zero value.

Oort 1992). This difference may be associated with the differences in eddy generation and propagation in the simulations compared to on Earth. For instance, midlatitude eddies preferentially propagate toward the equator on a sphere, whereas on a beta plane no such preference for the direction of eddy propagation exists. Additionally, stationary eddies play a large role in the momentum budget of Earth's atmosphere, particularly in the Northern Hemisphere (Caballero 2008), whereas in our zonally symmetric simulations, stationary eddies are practically absent. We present a more detailed comparison between the eddy momentum flux convergence in our wide-domain simulations and in Earth's atmosphere in the next section.

A further difference between the simulated and observed climate is that the wide-domain simulation exhibits equatorial westerlies in the upper troposphere, while the zonal wind in Earth's equatorial atmosphere is easterly. This superrotation is associated with equatorward fluxes of momentum by eddies at low latitudes (Fig. 2e). However, these features are absent in simulations using the gray-radiation scheme of O'Gorman and Schneider (2008) rather than Newtonian relaxation as the radiative parameterization, and for this reason we do not discuss them in detail here.

a. *Angular momentum transport*

Our simulations are conducted on an equatorial beta plane, and thus angular momentum, defined as the cross product of the linear momentum and a moment arm, is not conserved (e.g., Egger 2001). Nevertheless, we may define a scalar quantity that is conserved in the absence of eddies and behaves similarly to the angular momentum per unit mass in the direction of the rotation axis that is traditionally used in studies of the Hadley circulation in spherical geometry (e.g., Walker and Schneider 2006). The zonal momentum equation under the anelastic and beta-plane approximations may be written

$$\frac{\partial u}{\partial t} + u\frac{\partial u}{\partial x} + v\frac{\partial u}{\partial y} + w\frac{\partial u}{\partial z} = \beta y v - \frac{1}{\rho_0}\frac{\partial p}{\partial x} + F_x. \quad (4)$$

Here, (u, v, w) are the velocity components in the (x, y, z) directions, β is the gradient of the Coriolis parameter in the meridional direction, p is the perturbation pressure, F_x represents forces resulting from friction, and $\rho_0(z)$ is the reference density used in the anelastic approximation; it depends only on the vertical coordinate. Assuming a statistical steady state, we may take the zonal and time mean of the above equation to give

$$\overline{v}\left(\frac{\partial \overline{u}}{\partial y} - \beta y\right) + \overline{w}\frac{\partial \overline{u}}{\partial z} = -\frac{1}{\rho_0}\frac{\partial \rho_0 \overline{u'v'}}{\partial y} - \frac{1}{\rho_0}\frac{\partial \rho_0 \overline{u'w'}}{\partial z} + \overline{F_x}, \quad (5)$$

where the overbar represents a zonal and time mean and the primes a deviation thereof, and we have used the anelastic continuity equation $\nabla \cdot (\rho_0 \mathbf{u}) = 0$ to express the eddy terms in flux form. From (5), it may be seen that the quantity $M = \overline{u} - \beta y^2/2$ is conserved following the zonal-mean flow in the absence of eddies and frictional forces. We will refer to M as the angular momentum despite it not being defined as the cross product of the linear momentum with a moment arm.

Figure 4 shows the angular momentum, streamfunction, and mean saturation moist static energy for the case $\Delta T = 40$ K. In both the narrow- and wide-domain configurations, the HC includes a narrow ascending branch at the equator occupying a few degrees of latitude and a relatively broad descending branch. In the wide-domain simulation, streamlines of the flow regularly cross angular momentum contours, indicating substantial transport of angular momentum out of the HC by eddies. Additionally, the mean circulation includes a thermally indirect Ferrel cell that results from the generation of synoptic eddies at midlatitudes and their dissipation in the subtropics and subpolar regions. In the narrow-domain simulation, on the other hand, there is no Ferrel cell, and angular momentum is homogenized within the HC, indicating that the HC is relatively close to the angular momentum–conserving limit.

Since the narrow-domain simulation includes convective-scale eddies, the above results suggest that angular momentum transport by convection is relatively weak in

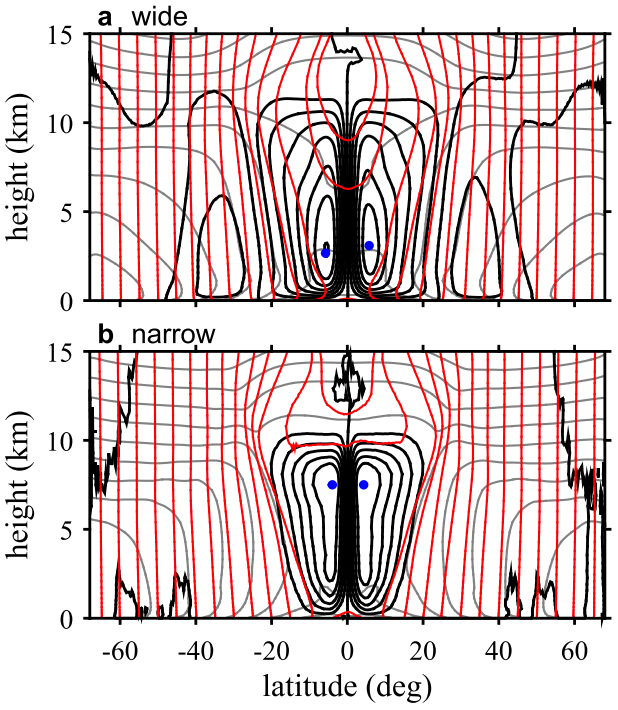

FIG. 4. Time-mean streamfunction Ψ (black), zonal- and time-mean angular momentum M (red), and zonal- and time-mean saturation moist static energy $\overline{h^*}$ (gray) in the (a) wide-domain simulation and (b) narrow-domain simulation with $\Delta T = 40$ K. The streamfunction is defined by (7) and is shown with contour intervals of 500 kg m^{-1} s^{-1}. The location of the streamfunction extremum in each hemisphere is marked by a blue dot. Contours are plotted for angular momentum values corresponding to the angular momentum of the surface at latitudes of 0°, ±5°, ±10°, etc. Saturation moist static energy is defined as $h^* = c_p T + \Phi + L_v q^*$, where q^* is the saturation specific humidity; contours are given for values at which $h^*/c_p = 280, 290, \ldots, 450$ K.

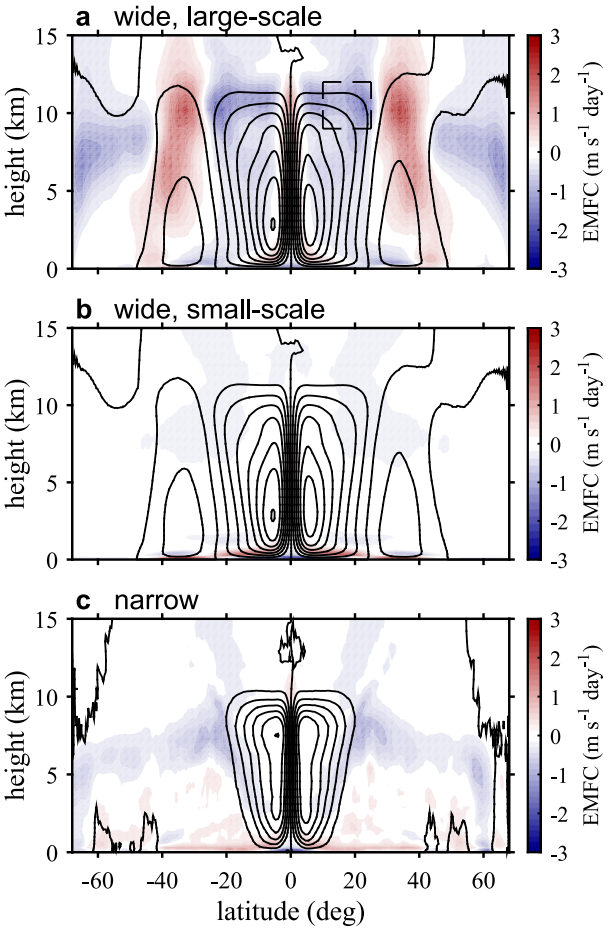

FIG. 5. EMFC (colors) and streamfunction (contours) in the (a),(b) wide-domain and (c) narrow-domain simulations with $\Delta T = 40$ K. EMFC associated with (a) large-scale eddies (wavelength > 960 km) and (b) small-scale eddies.

comparison to that of large-scale eddies. We confirm this conclusion by a direct calculation of the momentum flux convergence associated with eddies of different wavelengths below.

Figure 5 shows the eddy momentum flux convergence (EMFC), defined as

$$s = -\frac{1}{\rho_0}\frac{\partial \rho_0 \overline{u'v'}}{\partial y} - \frac{1}{\rho_0}\frac{\partial \rho_0 \overline{u'w'}}{\partial z}, \qquad (6)$$

in the wide- and narrow-domain cases for $\Delta T = 40$ K. In the wide-domain simulation, large-scale eddies (>960-km wavelength) act to decelerate the flow in the descending branch of the HC and accelerate it in the midlatitudes. While there is also some convergence of momentum directly over the equator associated with the weak superrotation noted previously, the simulated large-scale EMFC pattern is broadly similar to that of Earth's atmosphere during the equinoctial seasons [see Fig. 1 of Levine and Schneider (2011)].

To provide a more quantitative comparison, we calculate the mass-weighted mean of the large-scale horizontal EMFC between the latitudes of 10° and 25°N and between 9 and 12 km in altitude (dashed black box in Fig. 5a). This quantity has a value of -1.4 m s^{-1} day^{-1} in the wide-domain simulation for $\Delta T = 40$ K. A similar measure based on pressure levels between 200 and 300 hPa in the NCEP reanalysis is given in Fig. 2 of Caballero (2008); for the Northern Hemisphere during winter, this is approximately -2.8 m s^{-1} day^{-1} (summing the contributions from transient and stationary eddies). However, the Northern Hemisphere is strongly affected by stationary eddies, while in our zonally symmetric simulations, stationary eddies are of little importance. Performing a similar calculation for the Southern Hemisphere during spring gives a value

of $-1.8\,\mathrm{m\,s^{-1}\,day^{-1}}$, somewhat closer to the value in the wide-domain simulation.[1] These results indicate that the magnitude of the simulated EMFC for $\Delta T = 40\,\mathrm{K}$ is of the same order as, but somewhat smaller than, that of Earth's atmosphere. The reasons for the difference may be associated with the beta-plane geometry and zonal symmetry of our simulations, as mentioned above.

In contrast to the large-scale EMFC, eddies with wavelengths less than 960 km have a very weak effect on the flow above the boundary layer. While difficult to see in the contouring on Fig. 5b, small-scale eddies act to decelerate the upper-tropospheric flow in the subtropics, but this corresponds to a small fraction of the deceleration associated with large-scale eddies.

The magnitude of the small-scale EMFC in the wide-domain simulation may be quantified by calculating the Rayleigh damping time scale required to give the magnitude of the simulated EMFC, given the zonal wind speed. That is, we calculate τ assuming $s_s = -\overline{u}/\tau$, where s_s represents the small-scale EMFC. Theoretical studies of tropical convection often assume that convective momentum transport damps velocity anomalies over a time scale in the range 1–10 days (e.g., Romps 2014). In the simulations, however, the effective Rayleigh damping time scale in the subtropical mid- and upper troposphere is greater than 100 days. Only in the deep tropics, within the ITCZ, are there values of τ as short as a few days. The difference in time scales in these two regions may simply reflect the low frequency of occurrence of convection in the HC descending branch relative to the ITCZ. Convective momentum transport thus plays a very minor role in the momentum budget of our simulations, since, as postulated by Held and Hou (1980), the regions of strong vertical shear in which convective momentum transport may be expected to have the most effect are also regions in which convection is suppressed. This argument may be less applicable to nonequinoctial conditions, however, and we do not rule out a role for momentum transport by small-scale eddies in, for example, the seasonal migration of the ITCZ across the equator (Wu et al. 2003). A further caveat is that our equinoctial simulations do not form tropical cyclones, and this may affect the importance of convective momentum transport in the subtropics. Tropical cyclones form readily in simulations in which the ITCZ is displaced sufficiently far from the equator (see also Merlis et al. 2013), but the reason for their absence in the equinoctial simulations is unclear.

In the narrow-domain simulations, the EMFC is weaker than the corresponding wide-domain case, particularly within the HC (Fig. 5c). The small-scale eddies in the narrow-domain simulations primarily transport angular momentum vertically, damping the winds in the free troposphere. There is some deceleration of the flow in the HC descending branch, but, consistent with the limited crossing of angular momentum contours by streamlines in Fig. 4, this tendency is substantially weaker than in the wide-domain case.

b. Hadley circulation width

The poleward boundary of the HC is roughly demarcated by the outermost streamline associated with the HC shown on Fig. 4. In both the wide- and narrow-domain simulations, the HC width is close to 20° of latitude at upper levels, with the wide-domain HC extending slightly farther poleward. At low levels, however, the HC is considerably narrower in the narrow-domain case because streamlines of the descending branch are angled toward the equator; an air parcel initially at the poleward edge of the HC in the upper troposphere that follows streamlines on its descent would enter the boundary layer at a significantly lower latitude (<10°). In contrast, the descending branch of the wide-domain HC is closer to vertical, and the HC width at low levels is comparable to the HC width near the tropopause. These results are consistent with those of Satoh (1994) and S95.

The differences in the HC width described above may be understood by considering the axisymmetric theory of a moist HC outlined in Satoh (1994) and elaborated further by Fang and Tung (1996). Assuming a narrow region of ascent at the equator and conservation of angular momentum above the boundary layer, the authors derive an expression for the width of the HC given the distribution of SST. In the inviscid limit, angular momentum within the HC is homogenized to its value in the ascent region, and the surface pressure gradient is zero, preventing strong surface winds. As a result, the HC may only be in contact with the surface near the equator, where the angular momentum of the circulation matches that of the lower boundary. This implies that the HC width must be zero at the surface, and, as in the narrow-domain simulations, descending streamlines must slope downward toward the equator.

The assumption of angular momentum conservation implies, by the thermal wind relation, that horizontal temperature gradients are absent in the HC according to the Fang and Tung (1996) model. Consistent with this prediction, isotherms in the narrow-domain simulation are nearly horizontal within the HC (Fig. 6). Poleward of

[1] Here we follow Caballero (2008) and use data from the NCEP reanalysis (Kalnay et al. 1996) for the years 1962–99. We calculate the pressure-weighted mean of the horizontal EMFC between the latitudes of 10° and 25°S and pressure levels of 200 and 300 hPa for the spring season (SON).

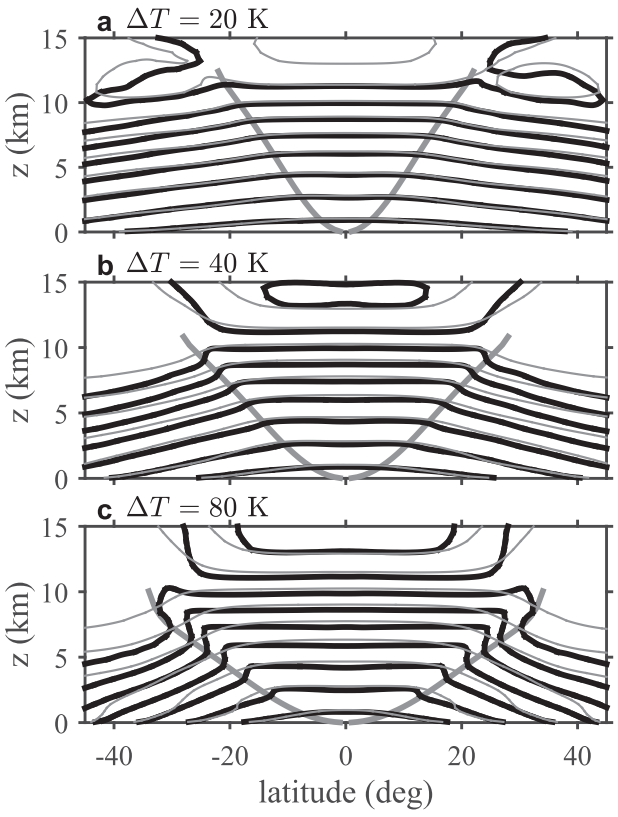

FIG. 6. Contours of zonal- and time-mean temperature in the narrow-domain (black) and wide-domain (thin gray) simulations with ΔT = (a) 20, (b) 40, and (c) 80 K. The thick gray line represents the boundary of the HC according to the axisymmetric theory of Fang and Tung (1996).

this, strong temperature gradients mark the boundary of the HC, and these regions of strong gradients correspond well to the sloping boundary predicted by the Fang and Tung (1996) model (thick gray lines). In Fig. 6, the functional form of the HC boundary is calculated using the continuity of the geopotential at a fixed pressure across the HC boundary. The geopotential within the HC is determined by geostrophic balance with the angular momentum–conserving wind. Outside the HC, the geopotential is related by hydrostatic balance to the temperature profile. Assuming the temperature profile within the HC follows a moist adiabat based on the equatorial surface temperature and the temperature profile outside the HC follows a moist adiabat based on the local surface temperature (with a surface relative humidity of 80% in both cases), expressions for the geopotential on either side of the HC boundary may be derived and the position of the HC boundary determined [see Fang and Tung (1996) for details].

When viscosity is added to the Fang and Tung (1996) model, air parcels in the descending branch no longer conserve their angular momentum, and the descending branch is no longer required to reach the surface near the equator. As a result, the HC boundary is altered so that the width of the HC increases incrementally at upper levels but by a large amount at lower levels (see their Fig. 3). The inclusion of viscosity in the axisymmetric model of Fang and Tung (1996) thus results in similar changes to the HC boundary as including large-scale eddies in our simulations. However, viscosity in an axisymmetric model is not completely analogous to the action of large-scale eddies; the torque provided by large-scale eddies occurs in the interior of the fluid as a result of primarily horizontal momentum transport, while viscosity primarily acts in boundary layers at the surface and HC boundary and transports momentum vertically. Additionally, it has been suggested that the HC extends to the latitude at which the depth of baroclinic eddies becomes comparable to the depth of the troposphere (Korty and Schneider 2008; Levine and Schneider 2015), which would suggest different mechanisms determine the HC extent in the wide- and narrow-domain simulations.[2] Nevertheless, the differences between the viscous and inviscid solutions in Fang and Tung (1996) provide some insight into the effect of eddy momentum transports on the slope of the HC boundary in our fixed-SST simulations.

c. *Hadley circulation strength*

We define the HC strength H as the maximum value of the symmetrized streamfunction $\Psi_{\text{sym}} = [\Psi(\phi) - \Psi(-\phi)]/2$, where Ψ is defined as[3]

$$\Psi = -\int_0^z \rho_0 \overline{v}\, dz' . \tag{7}$$

While other definitions of HC strength are possible, we focus on the streamfunction maximum because it is important for the precipitation rate in the ITCZ and because it is particularly relevant for evaluating the utility of the angular momentum–based perspective embodied in (1).

Despite the differently shaped streamlines, the strength of the HC is roughly equal between the wide- and narrow-domain simulations shown in Fig. 4. Indeed,

[2] Although it should be noted that in Levine and Schneider (2015) the criterion used to quantify the depth of baroclinic eddy fluxes depends on the near-surface temperature gradient, which, in our simulations, is constrained by the fixed-SST and does not depend strongly on the eddies.

[3] The streamfunction Ψ is expressed per unit length in the zonal direction rather than as a total mass overturning rate to enable comparison across the narrow- and wide-domain cases.

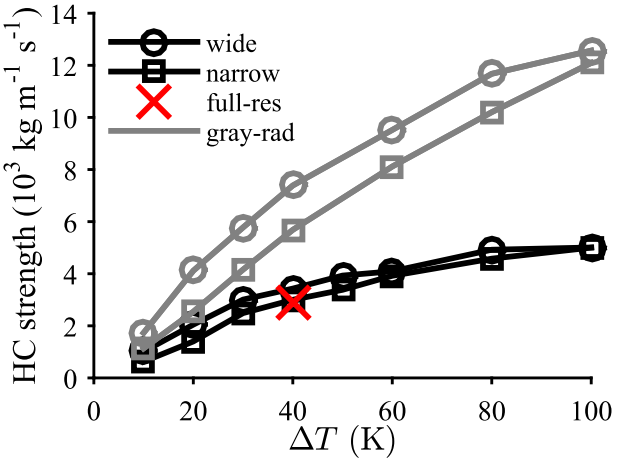

FIG. 7. Strength of the Hadley circulation as a function of the pole-to-equator SST difference ΔT in wide-domain (circles) and narrow-domain (squares) simulations. Simulations using the idealized radiation scheme based on Newtonian relaxation (black) and using the gray-radiation scheme (gray) are shown. The red cross shows the full-resolution, narrow-domain simulation. Hadley circulation strength is defined as the maximum value of the symmetric streamfunction Ψ_{sym} (see text).

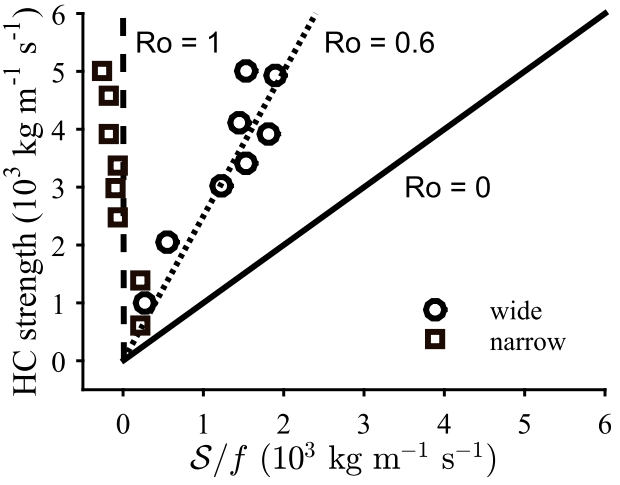

FIG. 8. HC strength plotted against $\mathcal{S}/f$ in wide-domain (circles) and narrow-domain (squares) simulations for ΔT values between 10 and 100 K. Lines show values of the bulk Rossby number of 0 (solid), 1 (dashed) and 0.6 (dotted). HC strength and $\mathcal{S}$ are calculated using zonal- and time-mean fields symmetrized about the equator, and we evaluate the integral in the definition of $\mathcal{S}$ at the latitude of the streamfunction maximum up to the level $z_t = 15$ km.

the HC strength scales with the pole-to-equator SST difference ΔT in a similar way with or without the influence of large-scale eddies (Fig. 7). This is also true for the gray-radiation simulations (gray lines), although in that case the narrow-domain HC is somewhat weaker than in the corresponding wide-domain simulation. S95 also reported similar HC strengths in 2D and 3D under fixed-SST conditions in a set of GCM simulations with varying planetary rotation rates.

In the limit in which the local Rossby number in the upper branch of the HC is small, the strength of the HC is constrained to respond proportionally to changes in eddy momentum flux divergence (e.g., Walker and Schneider 2006; Schneider and Bordoni 2008; Bordoni and Schneider 2010). This may be seen by integrating (5) vertically with mass weighting from the level of the maximum in the streamfunction z_m to the top of the Hadley circulation z_t, where the streamfunction vanishes to give

$$\int_{z_m}^{z_t} \rho_0 \overline{v} f (1 - \mathrm{Ro}_L)\, dz = \int_{z_m}^{z_t} \rho_0 \overline{w} \frac{\partial \overline{u}}{\partial z} dz - \int_{z_m}^{z_t} \rho_0 s\, dz, \quad (8)$$

where we have neglected torques due to friction. We may then define an appropriately weighted bulk Rossby number (Ro) such that

$$\Psi_{\max}(1 - \mathrm{Ro}) = \frac{\mathcal{S}}{f} + \frac{1}{f} \int_{z_m}^{z_t} \rho_0 \overline{w} \frac{\partial \overline{u}}{\partial z} dz, \quad (9)$$

where $\Psi_{\max}$ is the maximum value of the streamfunction at a given latitude and $\mathcal{S} = -\int_{z_m}^{z_t} \rho_0 s\, dz$. Evaluating the above equation at the latitude of the streamfunction maximum, $\Psi_{\max} = H$, where H is the HC strength, and the flow is quasi horizontal so that the second term on the right-hand side may be neglected. We are thus left with the simple relationship

$$H(1 - \mathrm{Ro}) \approx \frac{\mathcal{S}}{f}. \quad (10)$$

For small bulk Rossby number, the above equation relates the HC strength to the EMFC at the latitude of the streamfunction maximum. But for Rossby numbers of order unity, the HC strength may not be simply related to the eddy forcing.

Figure 8 shows the HC strength H plotted against $\mathcal{S}/f$ in the wide- and narrow-domain simulations. The ratio of these quantities gives an estimate of $1 - \mathrm{Ro}$ [noting the approximations made to derive (10)]. The bulk Rossby number in the narrow-domain simulations is close to unity, reflecting the weak influence of eddy momentum fluxes. In the wide-domain simulations, the Rossby number is substantially smaller; the differences in the eddy momentum flux divergence between the narrow- and wide-domain simulations are balanced by differences in Ro rather than differences in the strength of the overturning circulation.

The bulk Rossby number stays relatively constant at a value near 0.6 in the wide-domain simulations. This is

consistent with the behavior of the HC strength and the surface zonal wind speed at midlatitudes (a measure of the midlatitude EMFC), both of which increase with ΔT rapidly at low values of ΔT but remain relatively constant for $\Delta T \geq 60\,\mathrm{K}$ (Figs. 3 and 7). However, a bulk Rossby number of 0.6 is not close to the linear limit, and thus we should not necessarily expect the streamfunction maximum to vary in proportion to the eddy momentum flux divergence (see section 4).

d. *Thermodynamic estimate for the Hadley circulation strength*

Since the angular momentum–based perspective does not appear to provide a strong constraint on the strength of the HC, we appeal to thermodynamic considerations in order to obtain insight into the mechanisms at work. Analysis of the thermodynamic budget of the descending branch of the HC reveals that the leading-order balance is between vertical advection of potential temperature θ and the net diabatic heating rate Q_D:

$$\overline{w}\frac{\partial\overline{\theta}}{\partial z} = \overline{Q_D}. \tag{11}$$

This is a widely used approximation in tropical dynamics that is associated with the fact that horizontal gradients of temperature in the tropical free troposphere are constrained by wave dynamics to remain small (e.g., Charney 1963; Sobel et al. 2001; Holton 2004). Equation (11) relates the strength of the HC descent to the diabatic heating rate and the vertical gradient of potential temperature. In the free troposphere, the latter quantity would be expected to be relatively close to the potential temperature gradient along a moist adiabat. Furthermore, in our simple Newtonian-relaxation formulation, the radiative cooling rate only depends weakly on the atmospheric temperature structure and may also be considered as known. However, the diabatic heating rate also includes contributions from latent heating resulting from convection. The convective heating rate is sensitively dependent on the circulation, and for any complete theory of the HC, it must be a part of the solution.

The theoretical studies of Satoh (1994) and Fang and Tung (1996) close for the HC mass flux by considering the limit in which the HC descent is strong enough to shut off deep convection in the descending branch such that $Q_D \approx Q_R$, where Q_R is the radiative cooling rate. Under these conditions, we may use (11) to derive a thermodynamic estimate of the HC strength as follows. First, we define an estimated streamfunction Ψ^*. Using the continuity equation, the streamfunction given by (7) may be written in terms of the vertical velocity:

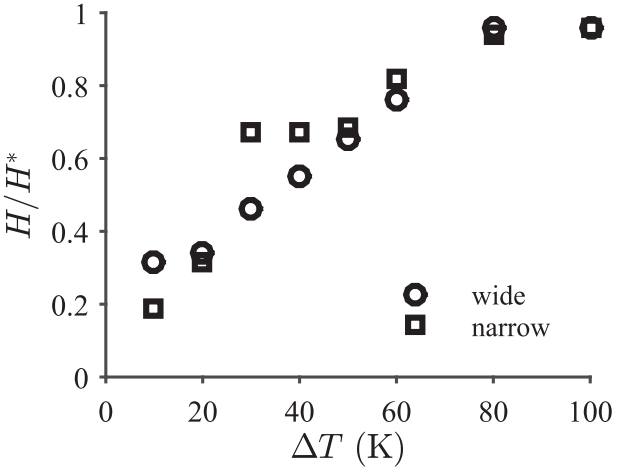

FIG. 9. Ratio of the simulated HC strength H to the HC strength estimated by assuming a radiative–subsidence balance in the descending branch H^* [see (13)] as a function of ΔT. Wide-domain simulations (circles) and narrow-domain simulations (squares) are shown.

$$\Psi(y,z) = \int_{-\infty}^{y} \rho_0 \overline{w}\, dy'. \tag{12}$$

The estimated streamfunction may then be found by replacing w in the above equation by the vertical velocity that satisfies a simple radiative-subsidence balance so that

$$\Psi^*(y,z) = -\mathrm{sign}(y)\int_{\zeta(z)}^{y} \frac{\rho_0 \overline{Q_R}}{\partial\overline{\theta}/\partial z}\, dy'. \tag{13}$$

Here, the integral is taken from the poleward boundary of the HC $\zeta(z)$ toward the equator. We calculate Ψ^* for latitudes between $\zeta(z)$ and the simulated streamfunction extremum and at heights above a nominal boundary layer of depth 1 km. For this calculation, we take $\zeta(z)$ as the location, at each height, for which the magnitude of the simulated streamfunction Ψ reaches 20% of its hemispheric maximum value (Ψ^* is only defined at levels for which the streamfunction reaches this 20% threshold). A threshold of 20% is used to eliminate noise in the calculated HC boundary, particularly at low values of ΔT for which the HC is relatively weak. Finally, since our definition of $\zeta(z)$ excludes 20% of the HC mass flux, we define the estimated HC strength H^* as the maximum value of Ψ^* divided by 0.8. For simplicity, the calculation of the estimated streamfunction is conducted using fields symmetrized between both hemispheres.

The HC strength estimated by the above procedure is too large relative to the simulated HC strength for all but the largest values of ΔT (Fig. 9). For low values of ΔT, convection has a substantial influence on the

thermodynamic balance in the subtropics, and the simulated HC strength is a small fraction (0.2–0.4) of that estimated by assuming a radiative-subsidence balance. As ΔT increases, the influence of convection decreases, until $\Delta T \geq 80\,\mathrm{K}$, at which point the estimated HC strength becomes a good approximation. However, this only occurs for values of ΔT larger than typical values of the pole-to-equator surface temperature difference on Earth. Indeed, Earth's annual-mean HC is estimated to be substantially weaker than the $\Delta T = 80$-K case shown here [e.g., Levine and Schneider (2011) give Earth's annual-mean HC strength as $\sim 11 \times 10^{10}\,\mathrm{kg\,s^{-1}}$, which is equivalent to $2.8 \times 10^{3}\,\mathrm{kg\,m^{-1}\,s^{-1}}$ at a latitude of 10°]. On the other hand, the winter HC is much stronger than the annual-mean case, and thus convection may be less important in the HC descent regions at certain times of the year. Nevertheless, our results suggest that predictions of the HC strength and its response to climate change based on a balance between radiative cooling and large-scale descent in the subtropics should be treated with caution.

While the thermodynamic considerations above do not allow for an accurate estimate of the HC strength, it should be noted that the importance of convection in the descending branch, as measured by the ratio of the simulated HC strength to the value estimated assuming no convective heating, is similar between the narrow- and wide-domain simulations as a function of ΔT. A heuristic argument for why this is the case may proceed as follows. The low-level temperature distribution in the simulations is set by the imposed SST distribution. Since temperature gradients within the Hadley circulation are relatively weak in both the narrow- and wide-domain cases, the upper-tropospheric temperature is largely determined by a moist adiabat originating in the ITCZ. The moist stability of columns in the HC descending branch is thus highly constrained under the fixed-SST boundary condition. If we postulate that the convective mass flux is a function of some measure of the gross stability of the column, this would result in an HC strength independent of the presence of eddies. This argument must be regarded as tentative, however, as it is unclear to what degree the convective mass flux may be thought of as solely a function of the mean atmospheric temperature structure. In particular, the moisture field may also be important for determining the frequency of convection in the HC descending branch, and the subtropical relative humidity is at least partially a function of the circulation itself. Additionally, near-surface temperature variability may be expected to enhance the ability of convection to penetrate the subtropical inversion, and such variability is considerably stronger in the wide-domain simulations. Despite these caveats, the rigidity of the temperature structure in our fixed-SST simulations likely contributes to the insensitivity of the HC strength to the presence of eddies.

4. Forced simulations

The simulations shown above remain relatively far from the low-Rossby-number regime that has been argued to be relevant for Earth's equinoctial HC, even in the wide-domain case. For this reason, we now investigate the response of the circulation to increasing eddy forcing strength, and thus decreasing Rossby number, by applying specified torques of various magnitudes to our simulations. Schneider (1984) used a similar method to study eddy influences on the HC in 2D simulations, but in that case the convective heating distribution was also specified. Here, convective heating is calculated explicitly by the model using the DARE approach.

We simulate the HC in the narrow-domain configuration with $\Delta T = 40\,\mathrm{K}$ while including an additional term in the prognostic equation for the zonal wind representative of the effect of eddies and given by

$$\left.\frac{\partial u}{\partial t}\right|_{\text{forcing}} = -\frac{F_u}{\rho_0}\frac{\partial}{\partial y}[\rho_0 \overline{u'v'}]_{\text{wide}}\,. \tag{14}$$

Here, the bracketed term on the right-hand side is the horizontal eddy momentum flux diagnosed from the wide-domain simulation with the same value of ΔT (given in Fig. 2e), and F_u is a scalar factor that we vary between 0 (no forcing) and 8. To remove small-scale noise, the diagnosed eddy momentum flux is smoothed with a five-point moving average in latitude and symmetrized between hemispheres before being applied to the forced simulations.

The imposed torques create sources and sinks of angular momentum in the upper troposphere that must be balanced by a combination of mean-flow advection, eddy momentum fluxes, and friction. In the narrow-domain simulations, eddy momentum fluxes are weak (except at very large forcing magnitudes), and thus the added momentum must be transported to the boundary layer by the mean circulation, where it can be removed by friction at the surface. This may be seen in Fig. 10; as the forcing amplitude is increased, the strength of the mean zonal surface wind also increases, implying a larger flux of momentum between the atmosphere and surface. For the case $F_u = 1$, the surface winds are similar to the wide-domain case, suggesting that the total convergence of angular momentum (including imposed torques) is similar in both cases.

The required angular momentum advection in the upper troposphere is achieved by a combination of a

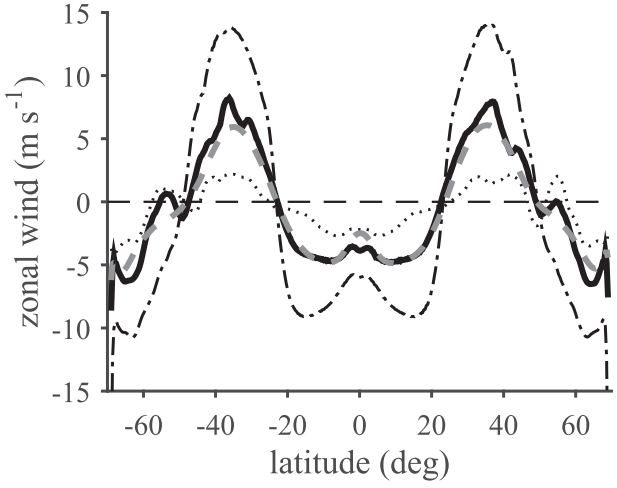

FIG. 10. As in Fig. 3, but for narrow-domain simulations forced with an applied torque proportional to the EMFC diagnosed from the corresponding wide-domain simulation. Forcing amplitudes of $F_u = 0.25$ (dotted), 1 (solid), and 4 (dashed–dotted) are shown for simulations with $\Delta T = 40$ K. The corresponding wide-domain simulation is shown as a dashed gray line.

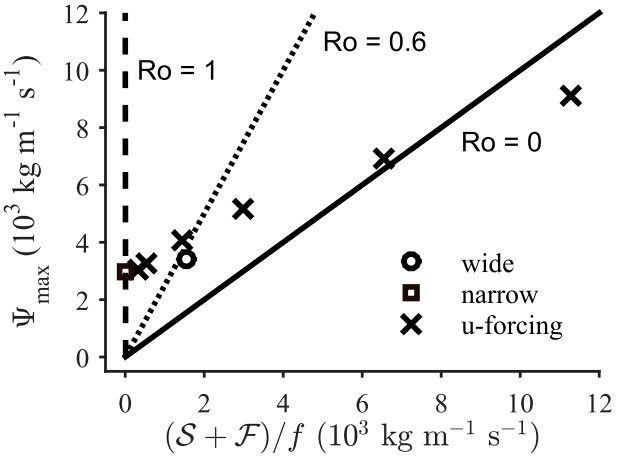

FIG. 11. As in Fig. 8, but for the streamfunction maximum Ψ_{max} and $(\mathcal{S}+\mathcal{F})/f$ evaluated at 10° latitude. Narrow-domain simulations with an applied torque proportional to the EMFC diagnosed from the corresponding wide-domain simulation (crosses) are shown with forcing amplitudes of $F_u = 0.25$, 0.5, 1, 2, 4, and 8 times the value in the wide-domain simulation. All simulations are conducted with $\Delta T = 40$ K, and the corresponding wide-domain simulation (circle) and narrow-domain simulation with no applied torque (square) are shown for comparison.

strengthening mean flow and increased gradients of angular momentum. As in the previous section, this may be analyzed in terms of the bulk Rossby number; for the forced simulations, (9) becomes

$$\Psi_{max}(1 - \mathrm{Ro}) = \frac{\mathcal{S}+\mathcal{F}}{f} + \frac{1}{f}\int_{z_m}^{z_t} \rho_0 \overline{w}\frac{\partial \overline{u}}{\partial z}\,dz, \qquad (15)$$

where $\mathcal{F}$ is the imposed momentum source integrated between z_m and z_t. Figure 11 shows Ψ_{max} plotted against $(\mathcal{S}+\mathcal{F})/f$ for the forced simulations. Here, we evaluate these quantities at 10° of latitude rather than at the latitude of the streamfunction maximum because the value of $\mathcal{F}$ changes sign near the streamfunction maximum, and the bulk Rossby number is not well defined there. The neglect of the vertical advection term is less justified at 10° of latitude compared with the location of the streamfunction maximum, but direct evaluation shows that the vertical advection term is of secondary importance, particularly when the imposed forcing is strong, and the dominant balance is between horizontal advection and the imposed momentum source. The ratio of Ψ_{max} and $(\mathcal{S}+\mathcal{F})/f$ may thus be taken as an estimate of $1 - \mathrm{Ro}$.

As the forcing amplitude F_u is increased, the bulk Rossby number decreases, and the strength of the overturning circulation increases relative to the no-forcing case. For moderate values of the forcing amplitude, the increase is relatively modest, but as the forcing increases beyond the magnitude of the eddy forcing in the wide-domain simulation, the circulation strengthens considerably. For $F_u = 4$, the streamfunction maximum is roughly double its value in the unforced narrow-domain simulation. Importantly, however, the HC strength does not respond proportionally to increases in the forcing amplitude, even for very strong forcing; part of the increase in forcing is balanced by decreases in the Rossby number, and the bulk Rossby number even becomes negative for $F_u = 8$.

In terms of the thermodynamic perspective, the increase in the strength of the overturning circulation with increasing F_u results primarily from an increase in the width of the HC in the low to midtroposphere at moderate values of the forcing. As the forcing is increased further, the circulation approaches the dry subtropical limit; for $F_u = 4$, the value of H/H^* calculated analogously to Fig. 9 is close to unity. Finally, at very high forcing strength ($F_u = 8$), the simulation develops strong eddy motions within the narrow domain, and the diabatic–subsidence balance given by (11) no longer holds.

A caveat regarding the forced simulations is that they do not include a full representation of the eddy–mean flow interaction, and thus they may develop unphysical mean flows. For instance, the HC strength for the case $F_u = 1$ is larger than in the corresponding wide-domain simulation (Fig. 11), and the forced simulation exhibits subtropical jets substantially stronger than in the wide-domain case (Fig. 12b). The jet strength is reduced somewhat when tendencies of temperature and moisture

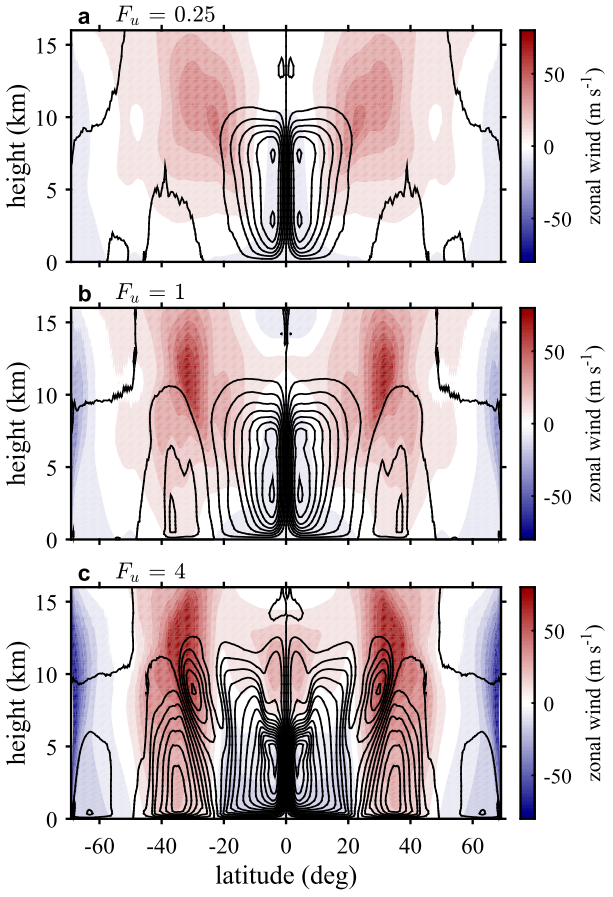

FIG. 12. Streamfunction (contours) and zonal- and time-mean zonal wind in narrow-domain simulations with $\Delta T = 40$ K. A torque is applied proportional to the EMFC diagnosed from the corresponding wide-domain simulation with amplitudes of (a) 0.25, (b) 1, and (c) 4 times the value in the wide-domain simulation.

due to eddies [and the associated vertical Eliassen–Palm fluxes (see Edmon et al. 1980)] are included in the forcing, but the discrepancy with the wide-domain case remains.

As the forcing strength is increased, the midlatitude jets intensify, while the zonal wind in the tropics and subtropics decreases (Fig. 12). For the case $F_u = 4$, the mean zonal wind in the region of the HC becomes easterly below 8 km, except in a region near the equator.[4] This implies that linear Rossby waves forming in midlatitudes would have difficulty propagating into the region of the HC. It would be likely that eddies propagating from the extratropics would therefore break before they reached the latitudes of the HC (Randel and Held 1991), and a forcing of such magnitude could not be maintained in a simulation in which the full eddy–mean flow interaction was represented.

Given the unrealistic mean flows in the forced simulations, their relevance at high-amplitude forcing may be questioned. Nevertheless, the lack of proportionality between the eddy forcing and HC strength warrants further investigation into the response of the HC to increasing eddy forcing. A more realistic approach would be to retain the full eddy–mean flow interaction and increase the intensity of the eddy field by manipulating the SST distribution or simply employing a midlatitude wave maker. Such extensions are beyond the scope of our present study, however, and they are left for future work.

5. Discussion and conclusions

Using idealized simulations on an equatorial beta plane, we have investigated the influence of eddies on the characteristics of the equinoctial Hadley circulation. The beta-plane configuration allows us to isolate the effect of large-scale eddies by comparing simulations run in a wide-domain configuration, in which large-scale eddies are present, to simulations run in a domain too narrow to permit synoptic-scale or planetary-scale disturbances. Additionally, our simulations include an explicit representation of convection, and they allow for an evaluation of the importance of convective momentum transport for the HC within the DARE framework.

We find that momentum transport by convective-scale eddies is relatively weak, and, as a result, the narrow-domain HCs are substantially closer to the angular momentum–conserving limit than in the corresponding wide-domain simulations. Despite this difference, the HC strength, as measured by the magnitude of the HC mass flux, is similar in the wide- and narrow-domain cases. To achieve comparable strength with weak eddy momentum fluxes, the narrow-domain simulations require a substantially higher bulk Rossby number, and they exhibit a descending branch that slopes downward toward the equator consistent with the axisymmetric model of Satoh (1994) and Fang and Tung (1996).

While the above results are consistent with S95, they appear to contrast with a number of other studies in which eddy momentum fluxes play a central role in determining the HC strength under equinox conditions (Walker and Schneider 2006; Schneider and Bordoni 2008). However, there are a number of differences between this previous work and the present study.

First, our simulations remain in a relatively large-Rossby-number regime, even in the case with large-scale

[4] The superrotating jet in the $F_u = 4$ simulations is a direct result of a convergence of zonal momentum in the equatorial upper troposphere that is present in the forcing (see Fig. 5a), and it does not appear if the forcing is altered to remove this feature (not shown).

eddies, and thus the balance in (1) is not as strong a constraint on the HC strength as in, for example, Walker and Schneider (2006). The high Rossby number in the HC simulations shown here may be partly a result of our use of beta-plane geometry; on a sphere, eddies forming in midlatitudes primarily propagate equatorward, whereas the beta plane does not exhibit such a bias in the direction of eddy propagation. For a given eddy amplitude, the effect on the HC would therefore be weaker on a beta plane. But Levine and Schneider (2015) recently conducted a GCM study of the HC over a wide range of climates and also found bulk Rossby numbers of 0.6 or greater in climates comparable to that of Earth and warmer, suggesting the use of a beta plane may not be the primary reason for this difference. Furthermore, the forced simulations shown in section 4 indicate that, even when the eddy forcing is increased substantially, the response of the HC strength need not be proportional to the momentum forcing amplitude. It should be noted, however, that the mean flows in the simulations with strong forcing are likely to be inconsistent with an eddy field that is forced by the propagation of midlatitude Rossby waves.

A second difference is that the present study, along with S95, makes use of a fixed-SST boundary condition. Walker and Schneider (2006) and Schneider and Bordoni (2008), on the other hand, use a thermal forcing that is a simple Newtonian relaxation with no surface. Importantly, the low-level atmospheric temperature is only weakly constrained in these studies, and the horizontal gradient of low-level temperature is allowed to vary substantially. In our simulations, the fixed SST provides a strong constraint on the low-level temperature, while the upper-level temperature within the Hadley circulation has weak meridional gradients because of the requirement that the zonal wind not exceed its angular momentum–conserving value. We argue that the relative rigidity of the temperature distribution under these conditions leads to the weak dependence of the HC strength on eddy momentum fluxes.

The importance of the fixed-SST boundary condition for the HC is also suggested by examining the net flux of energy from the atmosphere into the surface in simulations using the gray-radiation scheme (Fig. 13). In both the wide- and narrow-domain cases, there is a strong energy flux out of the surface in the subtropics and a weaker upward flux in the deep tropics. If we allowed the surface temperature to respond to such energy fluxes, this would result in a warming of the subtropical ocean relative to the deep tropics (i.e., a reduction in the meridional surface temperature gradient in the tropics). The magnitude of this surface flux pattern is substantially larger in the narrow-domain simulation,

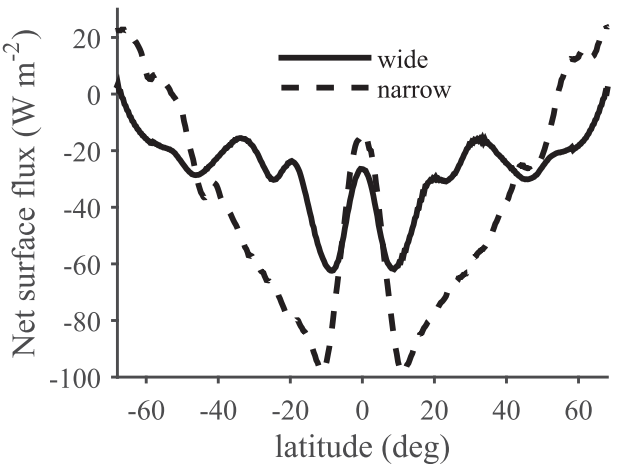

FIG. 13. Zonal- and time-mean surface flux (radiative and turbulent) in fixed-SST, gray-radiation simulations with $\Delta T = 40$ K in the wide (solid) and narrow (dashed) domains. Positive fluxes are directed into the surface.

suggesting a greater potential for a reduction of the meridional temperature gradient in that case. If, as our results suggest, the surface temperature distribution in the subtropics is an important determinant of the HC strength, the narrow-domain simulation would have a weaker HC when the SST is allowed to vary. Preliminary simulations using the gray-radiation scheme and a slab-ocean boundary condition confirm this picture. We will report on the results of the HC with a slab-ocean boundary condition in a separate paper.

While our results pertain to Hadley circulations that are relatively far from the low-Rossby-number limit and thus may not directly apply to Earth's equinoctial HC, they may nevertheless have implications for our understanding of the behavior of the HC under future climate change. For instance, the importance of convective heating in the descending branch of the circulation in our simulations suggests that predictions of the overturning circulation based on a radiative–subsidence balance in the subtropics should be treated with caution (cf. Ma et al. 2012). Furthermore, at the solstices, the HC deviates considerably from the low-Rossby-number regime, and understanding the HC at intermediate Rossby numbers may be important for understanding the factors influencing the strength of the global monsoon. Finally, the importance of the SST distribution in determining the HC strength in our simulations suggests that one should consider the energy budget, as well as the momentum budget, in order to understand the strength of the HC, particularly in the intermediate-Rossby-number regime. The energy transport by the HC depends, via the gross moist stability, on the detailed vertical structure of the circulation. For this reason, single-layer models of the HC

(e.g., Held and Hoskins 1985; Sobel and Schneider 2009) may be insufficient for this purpose.

Acknowledgments. The authors thank M. Khairoutdinov for access to the SAM code. Comments from I. Held and two anonymous reviewers helped to greatly improve an earlier version of this manuscript. Simulations used in this study were performed on the Harvard Odyssey cluster. This work was partially supported by NSF Grant AGS-1260380 and NASA Grant NNX13AN47G.

APPENDIX

Evaluation of the DARE Approach

We evaluate the validity of the DARE approach by comparing a simulation using DARE to one at full resolution. The full-resolution case is run with a horizontal grid spacing of 4 km and on a domain comprising 256×3840 grid points. Under DARE, we take $\gamma = 10$ and run with a horizontal grid spacing of 40 km on a domain comprising 24×384 grid points. Because of the large computational requirements of the full-resolution case, we only ran a single narrow-domain simulation in which $\Delta T = 40$ K.

In both the full-resolution and DARE cases, the circulation initially develops a double-ITCZ-like structure with two precipitation maxima on either side of the equator (Fig. A1). These maxima merge to form a single convergence region with propagating disturbances providing intermittent precipitation in subtropical regions. However, the time scale over which the simulations equilibrate is quite different between the DARE and full-resolution simulations. Under DARE, the two convergence zones merge around day 25, and the statistics of the zonal-mean precipitation rate appear to become stationary after ~50 days of model time. In the full-resolution simulation, a single ITCZ emerges after ~100 days, but it is unclear if the simulation has reached equilibrium even after 200 days of run time. The temporal variability in the precipitation rate is also different in the DARE case compared to the full-resolution case. For instance, there is an oscillation in the near-equatorial precipitation rate with a period of roughly 3 days in the DARE simulation that is absent in the full-resolution simulation.

Despite the differences outlined above, the mean circulations in the DARE simulation and full-resolution simulation are remarkably similar. Figure A2 shows the zonal- and time-mean properties of the full-resolution simulation calculated using 6-hourly snapshots over days 150–200. The streamfunction, angular momentum distribution, and saturation moist static energy distribution are very similar to the corresponding DARE simulation (shown in Fig. 4b). In both cases, the HC extends to roughly 20° latitude at upper levels but is substantially narrower near the surface. Additionally, angular momentum is homogenized in the HC region, indicating that the HC is close to the angular momentum–conserving limit. Finally, the HC strength is also almost identical in the full-resolution case compared to the DARE simulation (see red cross on Fig. 7). These results suggest that the DARE approach provides a good estimate of the characteristics of the mean flow when compared to a simulation at full resolution. Differences do arise when the temporal variability of the circulation is considered, but we leave detailed analysis of these differences to future work.

We also performed a simulation identical to the DARE case, but with $\gamma = 1$, in order to compare the DARE approach to simply using coarse resolution. The low-resolution simulation is similar to the DARE case, both in its mean state and variability (Fig. A1). As with the

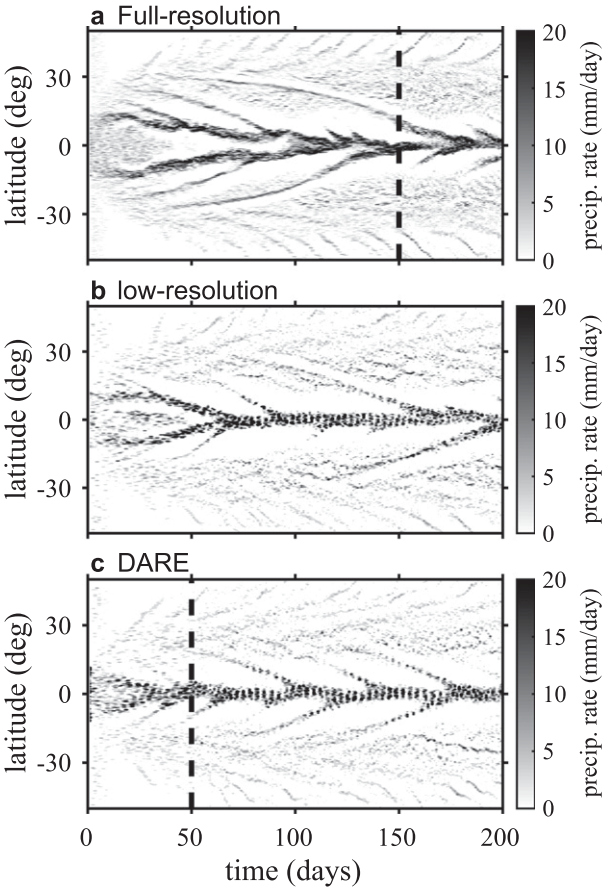

FIG. A1. Zonal- and daily mean precipitation rate as a function of time and latitude in narrow-domain simulations with $\Delta T = 40$ K. (a) Full-resolution simulation ($\gamma = 1$; horizontal grid spacing = 4 km), (b) low-resolution simulation ($\gamma = 1$; horizontal grid spacing = 40 km), and (c) DARE simulation ($\gamma = 10$; horizontal grid spacing = 40 km). Vertical dashed lines in (a) and (c) show the time after which statistics are collected in creating Figs. 2–13 and A2, respectively.

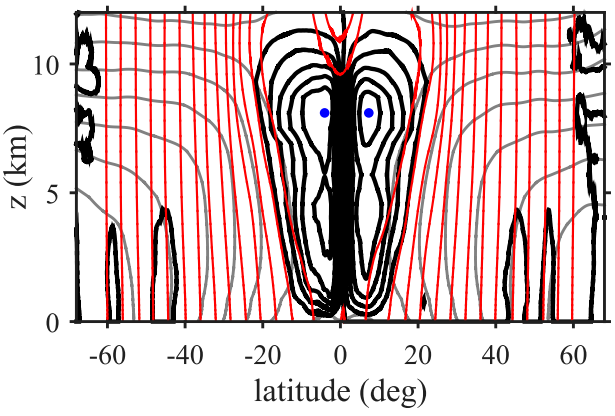

FIG. A2. As in Fig. 4b, but for the full-resolution simulation ($\gamma = 1$- and 4-km horizontal grid spacing).

DARE approach, the low-resolution simulation roughly reproduces the HC strength and mean circulation characteristics of the full-resolution simulation (not shown). Thus, the DARE approach does not appear to provide a significant advantage over coarse resolution in reproducing the full-resolution simulation. Nevertheless, we use the DARE approach in this paper, as it represents a physically realizable system in which the resolution is convection permitting (4-km grid spacing).

REFERENCES

Becker, E., G. Schmitz, and R. Geprägs, 1997: The feedback of midlatitude waves onto the Hadley cell in a simple general circulation model. *Tellus*, **49A**, 182–199, doi:10.1034/j.1600-0870.1997.t01-1-00003.x.

Bordoni, S., and T. Schneider, 2008: Monsoons as eddy-mediated regime transitions of the tropical overturning circulation. *Nat. Geosci.*, **1**, 515–519, doi:10.1038/ngeo248.

——, and ——, 2010: Regime transitions of steady and time-dependent Hadley circulations: Comparison of axisymmetric and eddy-permitting simulations. *J. Atmos. Sci.*, **67**, 1643–1654, doi:10.1175/2009JAS3294.1.

Caballero, R., 2007: Role of eddies in the interannual variability of Hadley cell strength. *Geophys. Res. Lett.*, **34**, L22705, doi:10.1029/2007GL030971.

——, 2008: Hadley cell bias in climate models linked to extra-tropical eddy stress. *Geophys. Res. Lett.*, **35**, L18709, doi:10.1029/2008GL035084.

——, R. T. Pierrehumbert, and J. L. Mitchell, 2008: Axisymmetric, nearly inviscid circulations in non-condensing radiative-convective atmospheres. *Quart. J. Roy. Meteor. Soc.*, **134**, 1269–1285, doi:10.1002/qj.271.

Charney, J. G., 1963: A note on large-scale motions in the tropics. *J. Atmos. Sci.*, **20**, 607–609, doi:10.1175/1520-0469(1963)020<0607:ANOLSM>2.0.CO;2.

Dickinson, R. E., 1971: Analytic model for zonal winds in the tropics. *Mon. Wea. Rev.*, **99**, 501–510, doi:10.1175/1520-0493(1971)099<0501:AMFZWI>2.3.CO;2.

Edmon, H. J., B. J. Hoskins, and M. E. McIntyre, 1980: Eliassen–Palm cross sections for the troposphere. *J. Atmos. Sci.*, **37**, 2600–2616, doi:10.1175/1520-0469(1980)037<2600:EPCSFT>2.0.CO;2.

Egger, J., 2001: Angular momentum of β-plane flows. *J. Atmos. Sci.*, **58**, 2502–2508, doi:10.1175/1520-0469(2001)058<2502:AMOPF>2.0.CO;2.

Eliassen, A., 1951: Slow thermally or frictionally controlled meridional circulation in a circular vortex. *Astrophys. Norv.*, **5**, 19–60.

Fang, M., and K. K. Tung, 1996: A simple model of nonlinear Hadley circulation with an ITCZ: Analytic and numerical solutions. *J. Atmos. Sci.*, **53**, 1241–1261, doi:10.1175/1520-0469(1996)053<1241:ASMONH>2.0.CO;2.

——, and ——, 1999: Time-dependent nonlinear Hadley circulation. *J. Atmos. Sci.*, **56**, 1797–1807, doi:10.1175/1520-0469(1999)056<1797:TDNHC>2.0.CO;2.

Held, I., and B. Hoskins, 1985: Large-scale eddies and the general circulation of the troposphere. *Advances in Geophysics*, Vol. 28, Academic Press, 3–31, doi:10.1016/S0065-2687(08)60218-6.

——, and A. Y. Hou, 1980: Nonlinear axially symmetric circulations in a nearly inviscid atmosphere. *J. Atmos. Sci.*, **37**, 515–533, doi:10.1175/1520-0469(1980)037<0515:NASCIA>2.0.CO;2.

Holton, J. R., 2004: *An Introduction to Dynamic Meteorology*. 4th ed. International Geophysics Series, Vol. 88, Academic Press, 535 pp.

Kalnay, E., and Coauthors, 1996: The NCEP/NCAR 40-Year Reanalysis Project. *Bull. Amer. Meteor. Soc.*, **77**, 437–471, doi:10.1175/1520-0477(1996)077<0437:TNYRP>2.0.CO;2.

Khairoutdinov, M. F., and D. A. Randall, 2003: Cloud resolving modeling of the ARM summer 1997 IOP: Model formulation, results, uncertainties, and sensitivities. *J. Atmos. Sci.*, **60**, 607–625, doi:10.1175/1520-0469(2003)060<0607:CRMOTA>2.0.CO;2.

Kim, H.-K., and S. Lee, 2001: Hadley cell dynamics in a primitive equation model. Part II: Nonaxisymmetric flows. *J. Atmos. Sci.*, **58**, 2859–2871, doi:10.1175/1520-0469(2001)058<2859:HCDIAP>2.0.CO;2.

Korty, R. L., and T. Schneider, 2008: Extent of Hadley circulations in dry atmospheres. *Geophys. Res. Lett.*, **35**, L23803, doi:10.1029/2008GL035847.

Krishnamurti, T. N., L. Stefanova, and V. Misra, 2013: *Tropical Meteorology: An Introduction.* Springer, 424 pp.

Kuang, Z., P. N. Blossey, and C. S. Bretherton, 2005: A new approach for 3D cloud-resolving simulations of large-scale atmospheric circulation. *Geophys. Res. Lett.*, **32**, L02809, doi:10.1029/2004GL021024.

Kuo, H.-L., 1956: Forced and free meridional circulations in the atmosphere. *J. Meteor.*, **13**, 561–568, doi:10.1175/1520-0469(1956)013<0561:FAFMCI>2.0.CO;2.

Levine, X. J., and T. Schneider, 2011: Response of the Hadley circulation to climate change in an aquaplanet GCM coupled to a simple representation of ocean heat transport. *J. Atmos. Sci.*, **68**, 769–783, doi:10.1175/2010JAS3553.1.

——, and ——, 2015: Baroclinic eddies and the extent of the Hadley circulation: An idealized GCM study. *J. Atmos. Sci.*, **72**, 2744–2761, doi:10.1175/JAS-D-14-0152.1.

Lindzen, R. S., and A. Y. Hou, 1988: Hadley circulations for zonally averaged heating centered off the equator. *J. Atmos. Sci.*, **45**, 2416–2427, doi:10.1175/1520-0469(1988)045<2416:HCFZAH>2.0.CO;2.

Ma, J., S.-P. Xie, and Y. Kosaka, 2012: Mechanisms for tropical tropospheric circulation change in response to global warming. *J. Climate*, **25**, 2979–2994, doi:10.1175/JCLI-D-11-00048.1.

Merlis, T. M., M. Zhao, and I. M. Held, 2013: The sensitivity of hurricane frequency to ITCZ changes and radiatively forced warming in aquaplanet simulations. *Geophys. Res. Lett.*, **40**, 4109–4114, doi:10.1002/grl.50680.

O'Gorman, P. A., and T. Schneider, 2008: The hydrological cycle over a wide range of climates simulated with an idealized GCM. *J. Climate*, **21**, 3815–3832, doi:10.1175/2007JCLI2065.1.

Pauluis, O., D. M. W. Frierson, S. T. Garner, I. M. Held, and G. K. Vallis, 2006: The hypohydrostatic rescaling and its impacts on modeling of atmospheric convection. *Theor. Comput. Fluid Dyn.*, **20**, 485–499, doi:10.1007/s00162-006-0026-x.

Peixoto, J. P., and A. H. Oort, 1992: *Physics of Climate.* AIP Press, 520 pp.

Randel, W. J., and I. M. Held, 1991: Phase speed spectra of transient eddy fluxes and critical layer absorption. *J. Atmos. Sci.*, **48**, 688–697, doi:10.1175/1520-0469(1991)048<0688:PSSOTE>2.0.CO;2.

Romps, D. M., 2014: Rayleigh damping in the free troposphere. *J. Atmos. Sci.*, **71**, 553–565, doi:10.1175/JAS-D-13-062.1.

Satoh, M., 1994: Hadley circulations in radiative–convective equilibrium in an axially symmetric atmosphere. *J. Atmos. Sci.*, **51**, 1947–1968, doi:10.1175/1520-0469(1994)051<1947:HCIREI>2.0.CO;2.

——, M. Shiobara, and M. Takahashi, 1995: Hadley circulations and their roles in the global angular momentum budget in two- and three-dimensional models. *Tellus*, **47A**, 548–560, doi:10.1034/j.1600-0870.1995.00104.x.

Schneider, E. K., 1977: Axially symmetric steady-state models of the basic state for instability and climate studies. Part II. Nonlinear calculations. *J. Atmos. Sci.*, **34**, 280–296, doi:10.1175/1520-0469(1977)034<0280:ASSSMO>2.0.CO;2.

——, 1984: Response of the annual and zonal mean winds and temperatures to variations in the heat and momentum sources. *J. Atmos. Sci.*, **41**, 1093–1115, doi:10.1175/1520-0469(1984)041<1093:ROTAAZ>2.0.CO;2.

——, and R. S. Lindzen, 1976: The influence of stable stratification on the thermally driven tropical boundary layer. *J. Atmos. Sci.*, **33**, 1301–1307, doi:10.1175/1520-0469(1976)033<1301:TIOSSO>2.0.CO;2.

——, and ——, 1977: Axially symmetric steady-state models of the basic state for instability and climate studies. Part I. Linearized calculations. *J. Atmos. Sci.*, **34**, 263–279, doi:10.1175/1520-0469(1977)034<0263:ASSSMO>2.0.CO;2.

Schneider, T., and S. Bordoni, 2008: Eddy-mediated regime transitions in the seasonal cycle of a Hadley circulation and implications for monsoon dynamics. *J. Atmos. Sci.*, **65**, 915–934, doi:10.1175/2007JAS2415.1.

Sobel, A. H., and T. Schneider, 2009: Single-layer axisymmetric model for a Hadley circulation with parameterized eddy momentum forcing. *J. Adv. Model. Earth Syst.*, **1** (10), doi:10.3894/JAMES.2009.1.10.

——, J. Nilsson, and L. M. Polvani, 2001: The weak temperature gradient approximation and balanced tropical moisture waves. *J. Atmos. Sci.*, **58**, 3650–3665, doi:10.1175/1520-0469(2001)058<3650:TWTGAA>2.0.CO;2.

Walker, C. C., and T. Schneider, 2005: Response of idealized Hadley circulations to seasonally varying heating. *Geophys. Res. Lett.*, **32**, L06813, doi:10.1029/2004GL022304.

——, and ——, 2006: Eddy influences on Hadley circulations: Simulations with an idealized GCM. *J. Atmos. Sci.*, **63**, 3333–3350, doi:10.1175/JAS3821.1.

Williams, G. P., 1988a: The dynamical range of global circulations–I. *Climate Dyn.*, **2**, 205–260, doi:10.1007/BF01371320.

——, 1988b: The dynamical range of global circulations–II. *Climate Dyn.*, **3**, 45–84, doi:10.1007/BF01080901.

Wu, X., X.-Z. Liang, and G. J. Zhang, 2003: Seasonal migration of ITCZ precipitation across the equator: Why can't GCMs simulate it? *Geophys. Res. Lett.*, **30**, 1824, doi:10.1029/2003GL017198.

Zhang, G. J., and N. A. McFarlane, 1995: Role of convective scale momentum transport in climate simulation. *J. Geophys. Res.*, **100**, 1417–1426, doi:10.1029/94JD02519.